

# Propagation Effects of Slanted Narrow Bipolar Events: A Rebounding-Wave Model Study

Dongshuai Li<sup>1,2</sup>, Alejandro Luque<sup>2</sup>, Farhad Rachidi<sup>3</sup>, Marcos Rubinstein<sup>4</sup>,  
Torsten Neubert<sup>1</sup>, Yanan Zhu<sup>5</sup>, Olivier Chanrion<sup>1</sup>, Caitano da Silva<sup>6</sup>,  
Paul R. Krehbiel<sup>6</sup>

<sup>1</sup>National Space Institute, Technical University of Denmark (DTU Space), Kongens Lyngby, Denmark.

<sup>2</sup>Instituto de Astrofísica de Andalucía (IAA), CSIC, Granada, Spain.

<sup>3</sup>Electromagnetic Compatibility Laboratory, Swiss Federal Institute of Technology (EPFL), Lausanne, Switzerland.

<sup>4</sup>University of Applied Sciences and Arts Western Switzerland, Yverdon-les-Bains, Switzerland.

<sup>5</sup>Earth Networks, Germantown, Maryland, USA.

<sup>6</sup>Langmuir Laboratory for Atmospheric Research, New Mexico Institute of Mining and Technology, Socorro, USA.

## Key Points:

- The propagation effect of slanted NBEs at different distance is investigated and compared with the observations.
- The inclination of the NBEs could significantly affect the electromagnetic fields in the close distance.
- The proposed equations will improve the quality of inferred features of slanted NBEs and can be extended to any discharge shape.

---

Corresponding author: Dongshuai Li<sup>1,2</sup> and Alejandro Luque<sup>2</sup>,

<sup>1</sup> National Space Institute, Technical University of Denmark (DTU Space), Kongens Lyngby, Denmark.

<sup>2</sup> Instituto de Astrofísica de Andalucía (IAA), CSIC, Granada, Spain., (dongshuai@space.dtu.dk, aluque@iaa.es)

**Abstract**

Narrow bipolar events (NBEs) are impulsive and powerful intracloud discharges. Recent observations indicate that some NBEs exhibit a slanted orientation rather than strictly vertical. However, the inclination of NBEs has not been considered in previous transmission line models, leading to uncertainty when evaluating their characteristics based on electromagnetic fields. This paper investigates the propagation effects of slanted NBEs using a newly developed slanted rebounding-wave model. It is found that the calculated results using the proposed model match well with measurements for both vertical and slanted NBE cases. The inclination of the NBEs significantly affects the electromagnetic fields at close distances, while the effects weaken as the observation distance increases, where the fields are dominated by the radiation component. The slanted rebounding-wave model improves the agreement with respect to a purely vertical channel and can be extended to any discharge geometry at arbitrary observation distances.

**Plain Language Summary**

Narrow Bipolar Events (NBEs) are unique intracloud discharges that occur either individually or as the initiation event for lightning flashes inside thunderstorms. Knowing the physical mechanisms of NBEs will help us to better understand how lightning initiates inside thunderstorms. Recent studies indicated that NBEs could exhibit a slanted orientation rather than being strictly vertical. Here, in the light of these observations, we analyze the propagation effect of the slanted NBEs by using a newly developed slanted rebounding-wave model, and we compare the modeling results with observations. This study contributes to a better understanding of the physical mechanism of NBEs and provides a reference for accurately characterizing NBEs based on their electromagnetic fields.

**1 introduction**

In recent years, significant attention has been given to Narrow Bipolar Events (NBEs) due to their important role in lightning initiation (Rison et al., 2016; Tilles et al., 2019; Lyu et al., 2019). NBEs are generated by the intracloud discharges that emit strong radiation in the high and very high frequency (HF/VHF) range (Le Vine, 1980; Smith et al., 1999, 2004), and they are characterized by fast breakdowns (FBs) that appear to be a system of streamer coronas (Rison et al., 2016; Phelps, 1974; Phelps & Griffiths, 1976; Attanasio et al., 2021; Tilles et al., 2019; Lyu et al., 2019; Attanasio et al., 2019). However, the exact physical mechanism behind NBEs still remains unclear.

The transmission line model is widely recognized as the most commonly used approach for inferring the characteristics of NBEs based on their electromagnetic fields. NBEs typically have channel lengths ranging from hundreds of meters to a few kilometers (Smith et al., 1999, 2004). When observing NBEs at distances as large as hundreds of kilometers, only the radiation field component is observable. Therefore, many studies simplify the NBE channel by assuming it to be an infinitesimally short dipole (Smith et al., 1999, 2004; Eack, 2004). This has led to misinterpretation of electric current intensities in all types of pulses taking place during the initial breakdown stage of lightning, as discussed by da Silva et al. (2016b). However, for close-range observations within a few kilometers or less, where induction and electrostatic fields are also significant, more accurate transmission line-based models of NBEs are proposed in the literature. These models include the classic transmission line (TL) model (Watson & Marshall, 2007), the modified transmission line with exponential increase (MTLEI) model (Watson & Marshall, 2007), the bouncing-wave transmission line model (Nag & Rakov, 2010), the modified transmission line with exponential decay (MTLE) model (Rison et al., 2016; Karunarathne et al., 2016) and the modified transmission line-gaussian (MTLG) model (da Silva et al., 2016a; R. A. Marshall et al., 2015). Attanasio et al. (2021) argued that, from an electrostatic standpoint, the precursor streamer system can produce a strong electric field enhancement ahead of itself that may trigger a rebounding opposite-polarity event traveling back towards the origin. Recently, Li, Luque, Gordillo-Vázquez, et al. (2022) introduced a rebounding-wave model based on the Modified Transmission Line with Exponential decay (MTLE) model (Nucci & Rachidi, 1989; Rachidi & Nucci, 1990; Rison et al., 2016), termed “rebounding MTLE model”, to represent the subsequent streamer features involved in NBEs (Rison et al., 2016;

69 Tilles et al., 2019; Attanasio et al., 2021). A common feature of all the transmission line-based  
70 models is the assumption that the NBE channel is vertically oriented.

71 Recent observations indicate that NBEs could be tilted from vertical and exhibit a noticeable  
72 spread in azimuthal values (Rison et al., 2016). Karunarathne et al. (2016) estimated the three-  
73 dimensional charge moments of ten NBEs and found that three of them were tilted at angles ranging  
74 from 10 to 20 degrees from the vertical. R. A. Marshall et al. (2015) suggested that slanted NBEs  
75 play a role in the illumination of the lower ionosphere known as “elve doublets”. Particularly, these  
76 authors suggested that if the NBE source current is inclined towards the observer, the second elve  
77 in the doublet can be brighter than the first. However, the impact of channel inclination on the  
78 propagation effects of NBEs at different distances remains unknown. Here, following previous stud-  
79 ies on the effect of the inclination and tortuosity of lightning return stroke channels (Le Vine &  
80 Meneghini, 1978b,a; Abouzeid & Zein El Dein, 2015), we propose an extension of the rebound-  
81 ing wave model of Li, Luque, Gordillo-Vázquez, et al. (2022) for NBEs. The so-called slanted  
82 rebounding wave model is firstly validated against a full-wave three-dimensional Finite-Difference  
83 Time-Domain (FDTD) method and then through comparisons with observations reported in the lit-  
84 erature.

## 85 2 Slanted rebounding wave model

86 The slanted transmission line model was firstly proposed by Abouzeid & Zein El Dein (2015)  
87 to analyze the effect of lightning return stroke channel tortuosity and branching. In this study, we  
88 extend their equations to investigate the inclination of the NBE channel. NBE is considered as a  
89 system of streamer coronas represented by the a rebounding-wave model based on the Modified  
90 Transmission Line with Exponential decay (MTLE) (Nucci & Rachidi, 1989; Rachidi & Nucci,  
91 1990; Rison et al., 2016), termed “rebounding MTLE model” (Li, Luque, Gordillo-Vázquez, et al.,  
92 2022).

93 As illustrated in Figure 1, the positive streamer coronas propagate downwards from an altitude  
94  $H_2$  to an altitude  $H_1$  with a channel length  $L$  (for a slanted channel  $H_1 = H_2 - r \cos \theta$ ), followed  
95 by upward negative streamer corona discharges that propagate back along the same path.  $I_d$  is the  
96 downward current (red color) and  $I_u$  is the rebounding-wave current (blue color). According to the  
97 rebounding MTLE model (Li, Luque, Gordillo-Vázquez, et al., 2022), the total current  $I(r, t)$  is the  
98 sum of the downward current  $I_d(r, t)$  and the upward rebounding current  $I_u(r, t)$ . Both currents are  
99 assumed to experience an exponential decay along the same propagation channel with attenuation  
100 rates of  $\lambda_d$  and  $\lambda_u$ , respectively. The total current and the downward and upward rebounding currents  
101 are given by

$$\begin{aligned} I(r, t) &= I_d(r, t) + I_u(r, t), \\ I_d(r, t) &= I(t - (L - r)/v_d)e^{-(L-r)/\lambda_d}, \\ I_u(r, t) &= I(t - L/v_d - r/v_u)e^{-L/\lambda_d}e^{-r/\lambda_u}, \end{aligned} \quad (1)$$

102 where  $v_d$  and  $v_u$  are the downward and upward propagation velocities. The factor  $e^{-L/\lambda_d}$  ensures the  
103 continuity between the downward and the upward-propagating currents.

104 In free space, the vertical electric field  $E_z$  at the observation point  $P(x_p, y_p, z_p)$ , where  $x_p =$   
105  $\rho \cos(\phi_p)$  and  $y_p = \rho \sin(\phi_p)$ , due to a short inclined dipole  $dr$  carrying the current  $I(r, t)$  located at a

106 height ( $H_2 - r \cos \theta$ ) is given as:.

$$dE_{zc} = -\frac{dr}{4\pi\epsilon_0} \left( \begin{array}{l} \left( \begin{array}{l} \frac{3(z_p - (H_2 - r \cos \theta))(x_p - r \sin \theta \cos \phi)}{R^5(r)} \sin \theta \cos \phi \\ + \frac{3(z_p - (H_2 - r \cos \theta))(y_p - r \sin \theta \sin \phi)}{R^5(r)} \sin \theta \sin \phi \\ + \frac{3(z_p - (H_2 - r \cos \theta))^2 - R^2(r)}{R^5(r)} \cos \theta \end{array} \right) \int_0^t I(r, t) d\tau \\ \left( \begin{array}{l} \frac{3(z_p - (H_2 - r \cos \theta))(x_p - r \sin \theta \cos \phi)}{cR^4(r)} \sin \theta \cos \phi \\ + \frac{3(z_p - (H_2 - r \cos \theta))(y_p - r \sin \theta \sin \phi)}{cR^4(r)} \sin \theta \sin \phi \\ + \frac{3(z_p - (H_2 - r \cos \theta))^2 - R^2(r)}{cR^4(r)} \cos \theta \end{array} \right) I(r, t) \\ \left( \begin{array}{l} \frac{(z_p - (H_2 - r \cos \theta))(x_p - r \sin \theta \cos \phi)}{c^2R^3(r)} \sin \theta \cos \phi \\ + \frac{(z_p - (H_2 - r \cos \theta))(y_p - r \sin \theta \sin \phi)}{c^2R^3(r)} \sin \theta \sin \phi \\ + \frac{(z_p - (H_2 - r \cos \theta))^2 - R^2(r)}{c^2R^3(r)} \cos \theta \end{array} \right) \frac{\partial I(r, t)}{\partial t} \end{array} \right), \quad (2)$$

107 where,

$$R(r) = \sqrt{(x_p - r \sin \theta \cos \phi)^2 + (y_p - r \sin \theta \sin \phi)^2 + (z_p - (H_2 - r \cos \theta))^2}. \quad (3)$$

108 Individual terms on the right hand side of Equation (2) containing the factors are the electrostatic,  
109 induction and radiation components. If we assume the ground as a perfectly conducting plane, its  
110 effect can be taken into account using image theory, yielding

$$dE_{zm} = -\frac{dr}{4\pi\epsilon_0} \left( \begin{array}{l} \left( \begin{array}{l} \frac{3(z_p + (H_2 - r \cos \theta))(x_p - r \sin \theta \cos \phi)}{R_0^5(r)} \sin \theta \cos \phi \\ + \frac{3(z_p + (H_2 - r \cos \theta))(y_p - r \sin \theta \sin \phi)}{R_0^5(r)} \sin \theta \sin \phi \\ - \frac{3(z_p + (H_2 - r \cos \theta))^2 - R_0^2(r)}{R_0^5(r)} \cos \theta \end{array} \right) \int_0^t I(r, t) d\tau \\ \left( \begin{array}{l} \frac{3(z_p + (H_2 - r \cos \theta))(x_p - r \sin \theta \cos \phi)}{cR_0^4(r)} \sin \theta \cos \phi \\ + \frac{3(z_p + (H_2 - r \cos \theta))(y_p - r \sin \theta \sin \phi)}{cR_0^4(r)} \sin \theta \sin \phi \\ - \frac{3(z_p + (H_2 - r \cos \theta))^2 - R_0^2(r)}{cR_0^4(r)} \cos \theta \end{array} \right) I(r, t) \\ \left( \begin{array}{l} \frac{(z_p + (H_2 - r \cos \theta))(x_p - r \sin \theta \cos \phi)}{c^2R_0^3(r)} \sin \theta \cos \phi \\ + \frac{(z_p + (H_2 - r \cos \theta))(y_p - r \sin \theta \sin \phi)}{c^2R_0^3(r)} \sin \theta \sin \phi \\ - \frac{(z_p + (H_2 - r \cos \theta))^2 - R_0^2(r)}{c^2R_0^3(r)} \cos \theta \end{array} \right) \frac{\partial I(r, t)}{\partial t} \end{array} \right), \quad (4)$$

111 where,

$$R_0(r) = \sqrt{(x_p - r \sin \theta \cos \phi)^2 + (y_p - r \sin \theta \sin \phi)^2 + (z_p + (H_2 - r \cos \theta))^2}. \quad (5)$$

112 For an observer P located on the ground surface, the height of the observation point  $z_p$  is equal  
113 to zero in all the equations above, implying  $R = R_0$ . The total vertical electric field  $E_z$  for the whole  
114 inclined channel can be obtained by integrating the dipole field  $dE_{zc}$  and its image  $dE_{zm}$  over the  
115 entire channel. Note that both the dipole field  $dE_{zc}$  and its image  $dE_{zm}$  include the slanted feature of  
116 the sources, and they reduce to the case of a vertical channel when the polar angle  $\theta = 0$  (Thottappillil  
117 & Rakov, 2001; M. A. Uman et al., 1975). Moreover, the equations are not limited to straight channel

but also can be applied to any arbitrarily tortuous discharge channel by approximating it as a series of small straight segments.

Although not mentioned in the study of Abouzeid & Zein El Dein (2015), the so-called discontinuity term (Thottappillil et al., 1998; Thottappillil & Rakov, 2001), “turn-on” term (M. A. Uman & McLain, 1970; M. A. Uman Martin A. & McLain, 1970) or F factor (Rubinstein & Uman, 1990; Thottappillil & Rakov, 2001, 2005; Shao et al., 2004, 2005) should be considered if there is a current discontinuity at the propagation wave front. The equations for the discontinuity term are given in Text S1 in Supporting Information.

### 3 Validation of the slanted rebounding wave model

To validate the proposed slanted transmission line equations for NBEs, we compare its prediction against a full-wave three-dimensional FDTD model (Li et al., 2016, 2017). In the simulation, the NBE source is assumed to be a dipole at an altitude  $H = 5$  km above a perfectly conducting ground with different polar angle  $\theta$  of  $0^\circ$ ,  $30^\circ$ ,  $60^\circ$  and  $90^\circ$ . The current waveform is given by double-exponential expression with  $I(t) = I_0(e^{\alpha t}/(1 + e^{(\alpha+\beta)t}))$ , where the rise time constant is  $\alpha = 1/\tau_1$  and the fall time constant is  $\beta = 1/\tau_2$  (Rison et al., 2016). The values of  $\tau_1$  and  $\tau_2$  are  $1 \mu\text{s}$  and  $5 \mu\text{s}$ , respectively. The peak current is normalized to  $I_{peak} = -100$  kA by setting  $I_0 = I_{peak}(1 + \frac{\alpha}{\beta})(\frac{\alpha}{\beta})^{\frac{1}{\alpha+\beta}}$ .

For a vertical dipole with  $\theta = 0^\circ$ , the electric field varies with azimuthal symmetry, but it is more complicated for the slanted cases showing different features depending on the different azimuthal angles. The comparison between the slanted rebounding wave model and the FDTD method for both vertical and slanted dipoles is given in Figure 2. The results calculated by the presented equations match perfectly with the FDTD results for both vertical and slanted sources. For horizontal dipole with  $\theta = 90^\circ$ , the electric field first increases within a distance of 5 km and then decreases as the observer moves away from the source and becomes negligible beyond a distance of about 50 km.

The results from the FDTD simulation are further shown in Figure S1 and S2 in Supporting Information. Figure S1 shows the side view (a, c, e, g) and top view (b, d, f, h) of a snapshot of the FDTD simulation for the vertical electric fields of the slanted dipole with  $\theta = 0^\circ$ ,  $30^\circ$ ,  $60^\circ$  and  $90^\circ$ . Figure S2 illustrates the electrostatic, induction and radiation components for both vertical and slanted dipoles at different distances. The inclination of the source at closer distances ( $\leq 10$  km) causes a significant effect on the electrostatic and induction components of the electric fields. Both the waveshape and the amplitude of the electric field are influenced by the inclination of the source (see Figure S2(d1, d2, d3)). In our case, the reversal distance (Nag & Rakov, 2010), where the electrostatic and induction components of the field reverse their polarity, varies as a function of the slanted dipole angle. As shown in Figure S2(d2, e2, d3 and e3), the tail part of the waveform becomes higher due to the increase of the electrostatic fields caused by the slant angle. For distances beyond 50 km, the electric field is dominated by the radiation component, and the inclination only affects the amplitudes (see Figure S2(d4 and e4)). It is interesting to note that the effect of the slant angle lower than  $30^\circ$  becomes weak beyond a distance of about 10 km. However, the effect of slant angles bigger than  $30^\circ$  could not be ignored even at distances as large as 50 km.

## 4 Comparison with the observations in the literature

### 4.1 The electrical discharges following NBEs

Recent studies reported that the electric fields of NBEs at distances below 10 km include two parts: a main bipolar pulse characteristic of NBE and a slow electrostatic change lasting from tens of microseconds to a few milliseconds (Karunaratne et al., 2016; T. Marshall et al., 2014). The slow electrostatic change following NBEs seems to be related to the attempted electrical activities that never developed into a full lightning flash (Karunaratne et al., 2016). This fact is also supported by the multi-pulse corona discharges observed by the Atmosphere-Space Interactions Monitor (ASIM) onboard International Space Station (ISS) (Li, Luque, Lehtinen, et al., 2022; Li et al., 2023). In their study, Li, Luque, Lehtinen, et al. (2022) found that, for the multi-pulse corona discharges, the first

166 optical pulse coincides with a strong radio signal in the form of a NBE but subsequent optical pulses,  
 167 delayed by some milliseconds, are related to horizontally oriented streamer-like electrical discharges  
 168 which do not trigger full-fledged lightning. However, it remains unclear whether these electrical dis-  
 169 charges following NBEs are part of the NBEs produced by the remaining streamer corona activities  
 170 (Rison et al., 2016; Li, Luque, Gordillo-Vázquez, et al., 2022) or if they are independent electrical  
 171 discharges, similar to the Initial E-Change (IEC) that occurs before the first initial breakdown pulses  
 172 of a lightning flash (T. Marshall et al., 2014, 2019; Kostinskiy et al., 2020).

173 In our study, we consider these electrical discharges as an extra long decay current  $I_{extra}$  along  
 174 with the main NBE current, despite lacking knowledge about their physical mechanism. The current  
 175 is represented using the double-exponential expressions (Rison et al., 2016),

$$I(t) = I_{NBE}(t) + I_{extra}(t) = I_0 \frac{e^{\alpha t}}{1 + e^{(\alpha+\beta)t}} + \eta I_0 \frac{e^{\alpha t}}{1 + e^{(\alpha+\gamma)t}}, \quad (6)$$

176 where the rise time constant for the original streamer current  $\alpha = 1/\tau_1$  and the fall time constant for  
 177 the original streamer current  $\beta = 1/\tau_2$ . For the extra current  $\gamma = 1/\tau_3$ .  $0 \leq \eta \leq 1$  is the fraction of  
 178 the extra current  $I_{extra}(t)$  compared to the primary NBE current  $I_{NBE}(t)$ . The peak value of  $I_{NBE}$   
 179 is normalized to  $I_{peak}$  by setting  $I_0 = I_{peak}(1 + \frac{\alpha}{\beta})(\frac{\alpha}{\beta})^{(\frac{\alpha}{\alpha+\beta})}$ .

#### 180 4.2 Comparison with the observations reported by Rison et al. (2016)

181 In this section, we compare the simulated results obtained by the slanted rebounding wave  
 182 model with the electric fields measured by a fast antenna (FA) for the vertical and slanted cases re-  
 183 ported by Rison et al. (2016). According to interferometer (INTF) observations, the NBEs consisted  
 184 of a downward Fast Positive Breakdown (FPB) followed immediately by an upward Fast Negative  
 185 Breakdown (FNB) that propagated back in the opposite direction along the previous path. In the  
 186 simulation, we model the fast breakdown of the NBE as a system of positive streamers that propa-  
 187 gate downwards over a distance  $L$ , then upwards back along the previous path as predicted by the  
 188 rebounding MTLE model (Li, Luque, Gordillo-Vázquez, et al., 2022). The same double-exponential  
 189 current is adopted for the comparison with the results of Rison et al. (2016).

190 According to Equation (1), the total current  $I(r, t)$  is the sum of the downward current  $I_d(r, t)$   
 191 and the upward rebounding current  $I_u(r, t)$ , where  $v_d = L/t_d$  and  $v_u = L/t_u$  are the downward and  
 192 upward velocities related to the inferred downward and upward propagation times  $t_d$  and  $t_u$  obtained  
 193 by fitting the INTF traces for both NBE1 and NBE3 with the best fit lines shown in Li, Luque,  
 194 Gordillo-Vázquez, et al. (2022) (see Figure 2 there).

195 As mentioned by Rison et al. (2016), the NBE1 discharge occurred at constant azimuth con-  
 196 sistent with the positive breakdown being vertically downward (see Figure 7 in the Supplementary  
 197 Material of Rison et al. (2016)). On the other hand, NBE3 showed substantial azimuthal spread with  
 198 nonnegligible tilt from vertical (see Figure 9 in the Supplementary Material of Rison et al. (2016)).  
 199 Firstly, we assume the channel to be vertical ( $\theta = 0$ ) for both NBE1 and NBE3. Note that the results  
 200 by assuming both NBE1 and NBE3 to be vertical are discussed in Li, Luque, Gordillo-Vázquez, et  
 201 al. (2022). Here we also present the results in Figure 3 with the best-fit parameters listed in Table S1  
 202 in Supporting Information. The estimated charge moment change  $Q_{mom}$  for the vertical NBE1 and  
 203 vertical NBE3 are  $-215 \text{ C} \cdot \text{m}$  and  $-116 \text{ C} \cdot \text{m}$ , respectively. It is found that the simulated results for  
 204 NBE1 agree well with the observations. However, this is not the case for the slanted case of NBE3,  
 205 for which significant deviations can be observed, especially in the tail part of the waveform.

206 In order to investigate the effect of the inclination of NBE sources on the fields, we introduce  
 207 an additional free parameter, the polar angle  $\theta$ , to represent the effect of inclination. To simplify  
 208 the geometry, we assume that the plane containing the NBE channel is perpendicular to the transfer  
 209 vector from the INTF observations' geometry to the geometry used in Figure 1 (see Text S2 and  
 210 Figure S3 in Supporting Information). The azimuth angle for the source  $\phi = 249^\circ$  and for the  
 211 observation point  $P$ ,  $\phi_p = 160^\circ$ , are estimated based on the transformation. The simulated result  
 212 for the slanted NBE3 is presented in Figure 3(c) with the inferred features shown in Table S1 in  
 213 Supporting Information. By considering the simulation-estimated polar angle of  $\theta = 15^\circ$ , the

214 simulated waveform for NBE3 reasonably agrees with the measurement, corresponding to a charge  
 215 moment change of  $-357 \text{ C} \cdot \text{m}$ , which is three times larger than the vertical case. However, the  
 216 observed flattening tail part of NBE3 still could not be matched well. This suggests that NBE3  
 217 might involve more complicated processes than just being slanted.

218 As mentioned earlier, the electrostatic offset of NBE3 could be produced by the remaining  
 219 streamer activities following NBEs (Rison et al., 2016). To address this, we introduce an additional  
 220 long decay current,  $I_{extra}$ , derived from the presence of the remaining streamer corona activities of  
 221 NBE3 that last for a few microseconds (see the subsequent signals at  $20 \mu\text{s} - 50 \mu\text{s}$  of Figure 2(b) in  
 222 Rison et al. (2016)). The results in Figure 3(d) show that by considering the extra long decay current  
 223  $I_{extra}$  and the simulation-estimated angle  $\theta = 15^\circ$  with respect to the z-axis, the tail parts of the  
 224 electrostatic and induction components for NBE3 have been reduced, resulting in a better agreement  
 225 with the observation (see Figure 3(b) and (d)). In this case, the estimated charge moment change  
 226  $Q_{mom}$  of the NBE3 is  $-219 \text{ C} \cdot \text{m}$ , which is similar to that of vertical NBE1.

227 Figure S4 in Supporting Information further shows the current distribution along the channel  
 228 based on the rebounding MTLE model for the vertical NBE1, the vertical NBE3, and the slanted  
 229 NBE3 without and with the extra current  $I_{extra}$ . We see that, among all cases, considering the inclina-  
 230 tion of the channel and the extra long decay current  $I_{extra}$  results in the best agreement with the INTF  
 231 traces. This is consistent with the observations showing substantial azimuthal spread indicating a  
 232 tilted channel.

### 233 4.3 Comparison with the observations reported by Karunarathne et al. (2016)

234 In this section, we compare the simulated results obtained by the slanted rebounding wave  
 235 model with the electric fields measured by a FA array for the vertical and slanted cases reported by  
 236 Karunarathne et al. (2016). In their study, Karunarathne et al. (2016) estimated three-dimensional  
 237 charge moments of ten NBEs based on a dipole model and found that seven NBEs were essentially  
 238 vertically oriented, while three NBEs were tilted at angles ranging from 10 to 20 degrees from the  
 239 vertical. To further investigate the effect of the inclination in the NBE channel, we have chosen two  
 240 cases: (i) NBE#174 corresponding to a vertical channel, and (ii) NBE#92 corresponding to a tilted  
 241 channel.

242 Similar to the previous simulations, we consider the fast breakdown of NBEs as a system of  
 243 positive streamers that propagate downwards along a distance  $L$ , then upwards back along the previ-  
 244 ous path, following the rebounding MTLE model (Li, Luque, Gordillo-Vázquez, et al., 2022). Since  
 245 the fast breakdowns for both NBE#174 and NBE#92 are followed by slow electrostatic changes, in  
 246 the simulation, we add the extra long decay current  $I_{extra}$  to address the effect of these slow electro-  
 247 static changes according to Equation (6).

248 As shown in Figure 4, for the vertical case NBE#174, with a polar angle  $\theta = 0^\circ$ , the simulated  
 249 results considering the extra long decay current  $I_{extra}$  agree well with the electric fields measured by  
 250 different fast antennas located at distances from 9 km to 70 km. To compare our modeling results  
 251 with those of Karunarathne et al. (2016), we assumed a channel length of 1000 m and a propagation  
 252 velocity of  $v = 2.6 \times 10^7 \text{ m/s}$ , both taken from the literature (Rison et al., 2016; Karunarathne et al.,  
 253 2016). The best-fit parameters listed in Table S1 in Supporting Information are consistent with those  
 254 reported by Karunarathne et al. (2016). It is worth noting that although Karunarathne et al. (2016)  
 255 modeled NBE#174 in their study, they were unable to accurately reproduce the slow electrostatic  
 256 changes at close stations since they assumed a current for the slow electrostatic change that linearly  
 257 decreases with time. However, in our case, the observed electrostatic change can be explained by  
 258 introducing an extra current  $I_{extra}$  that follows a double-exponential expression, which suggests that  
 259 the current of the electrostatic change may actually decrease exponentially, rather than linearly.

260 The results illustrated in Figure 5(a,c,e,g) indicate that by assuming a vertical channel for the  
 261 slanted case of NBE#92, the simulation does not agree well with the tail part of the observations at  
 262 close distances, but shows a reasonable agreement beyond a distance of about 10 km. As previously  
 263 mentioned, this is likely due to the inclination of the NBE sources, as supported by the results

264 shown in Figure 5(b,d,f,h). From Figure 5, we see that when the simulation-estimated angle  $\theta =$   
 265  $13^\circ$  with respect to the Z axis is taken into account, the modeling of the tail part corresponding  
 266 to the electrostatic component improves, resulting in a better agreement with both close and far  
 267 observations.

268 The current distribution based on the rebounding MTLE model for the vertical NBE#174, the  
 269 vertical NBE#92 and the slanted NBE#92 are given in Figure S5 in Supporting Information with  
 270 the detailed inferred parameters given in Table S1 in Supporting Information. The model-estimated  
 271 charge moment  $Q_{\text{mom}}$  for NBE#92 changed from  $-4519 \text{ C} \cdot \text{m}$  to  $-6958 \text{ C} \cdot \text{m}$  when considering the  
 272 vertical channel instead of the slanted channel. Although our rebounding-wave model is capable of  
 273 modeling the rebounding features inside the waveform, the rebounding wave feature for NBE#92 is  
 274 not obvious due to the strong downward attenuation rate  $\lambda_d$ .

## 275 **5 conclusions**

276 In this study, we investigated the propagation effect of slanted NBE sources by using a new  
 277 rebounding-wave model based on the slanted transmission line model. The modeling results were  
 278 first validated against the full-wave FDTD method, and then compared with the observations for  
 279 both vertical and slanted cases reported in the literature.

280 The inclination of the NBE channel significantly affects the electrostatic, induction, and ra-  
 281 diation components of the electric fields at close distances ( $d < 10 \text{ km}$ ). However, the effect gets  
 282 weaker at far distances ( $d > 50 \text{ km}$ ) where the fields are dominated by the radiation component. The  
 283 effect of an inclination less than  $30^\circ$  becomes weak beyond a distance of about 10 km. However,  
 284 the effect of slant angles bigger than  $30^\circ$  can not be ignored even at a distance of 50 km. For all the  
 285 slanted cases, the proposed model considering the channel inclination improves the agreement with  
 286 respect to a purely vertical channel.

287 Additionally, the effect of the slow electrostatic change following the NBEs was discussed. The  
 288 results that consider the extra long decay current based on a double-exponential expression match  
 289 well with the slow electrostatic change in both close and far observations. This suggests that the  
 290 current of the slow electrostatic change may actually decrease exponentially, rather than linearly.

291 Apart from the NBE cases discussed in this study, the suggested equations can be applied to  
 292 arbitrary observation distances, and, by approximating a curved channel geometry with piecewise  
 293 linear segments, it can be further extended to any discharge shape.

## 294 **Acknowledgments**

295 The authors would like to thank Dr. Thomas C. Marshall, Dr. Sumedhe Karunarathne and Dr.  
 296 Maribeth Stolzenburg at the University of Mississippi for providing data from Karunarathne et al.  
 297 (2016). This work was supported by the European Research Council (ERC) under the European  
 298 Union H2020 programme/ERC grant agreement 681257. Additionally, this work was supported by  
 299 the Spanish Ministry of Science and Innovation, MINECO, under the project PID2019-109269RB-  
 300 C43 and FEDER program. D.L. would like to acknowledge the Independent Research Fund Den-  
 301 mark (Danmarks Frie Forskningsfond) under grant agreement 1026-00420B. D.L., A.L. and F.J.G.V.  
 302 acknowledge financial support from the State Agency for Research of the Spanish MCIU through  
 303 the 'Center of Excellence Severo Ochoa' award for the Instituto de Astrofísica de Andalucía (SEV-  
 304 2017-0709).

## 305 **Open Research**

306 The data that support the findings of this study are openly available in [https://doi.org/](https://doi.org/10.5281/zenodo.8069595)  
 307 [10.5281/zenodo.8069595](https://doi.org/10.5281/zenodo.8069595).

## References

- Abouzeid, G., Said I. and Shabib, & Zein El Dein, A. (2015). Analysis of Electromagnetic Fields Generated by Inclined Lightning Channel. *Arabian Journal for Science and Engineering*, 40(9), 2585–2608. doi: 10.1007/s13369-015-1660-7
- Attanasio, A., da Silva, C., & Krehbiel, P. (2021). Electrostatic Conditions That Produce Fast Breakdown in Thunderstorms. *Journal of Geophysical Research: Atmospheres*, 126(19), e2021JD034829. doi: <https://doi.org/10.1029/2021JD034829>
- Attanasio, A., Krehbiel, P. R., & da Silva, C. L. (2019). Griffiths and Phelps Lightning Initiation Model, Revisited. *Journal of Geophysical Research: Atmospheres*, 124(14), 8076-8094. doi: 10.1029/2019JD030399
- da Silva, C. L., Merrill, R. A., & Pasko, V. P. (2016a). Mathematical constraints on the use of transmission line models to investigate the preliminary breakdown stage of lightning flashes. *Radio Science*, 51(5), 367-380. doi: <https://doi.org/10.1002/2015RS005853>
- da Silva, C. L., Merrill, R. A., & Pasko, V. P. (2016b, May). Mathematical constraints on the use of transmission line models to investigate the preliminary breakdown stage of lightning flashes. *Radio Science*, 51(5), 367–380. doi: 10.1002/2015RS005853
- Eack, K. B. (2004). Electrical characteristics of narrow bipolar events. *Geophysical Research Letters*, 31(20). doi: 10.1029/2004GL021117
- Karunarathne, S., Marshall, T. C., Stolzenburg, M., & Karunarathna, N. (2016). Electrostatic field changes and durations of narrow bipolar events. *Journal of Geophysical Research: Atmospheres*, 121(17), 10,161-10,174. doi: <https://doi.org/10.1002/2016JD024789>
- Kostinskiy, A. Y., Marshall, T. C., & Stolzenburg, M. (2020). The Mechanism of the Origin and Development of Lightning From Initiating Event to Initial Breakdown Pulses (v.2). *Journal of Geophysical Research: Atmospheres*, 125(22), e2020JD033191. doi: <https://doi.org/10.1029/2020JD033191>
- Le Vine, D. M., & Meneghini, R. (1978a, May). Electromagnetic fields radiated from a lightning return stroke: Application of an exact solution to Maxwell's equations. , 83(C5), 2377-2384. doi: 10.1029/JC083iC05p02377
- Le Vine, D. M., & Meneghini, R. (1978b, sep). Simulation of radiation from lightning return strokes: The effects of tortuosity. *Radio Science*, 13(5), 801-809. doi: 10.1029/RS013i005p00801
- Le Vine, D. M. (1980). Sources of the strongest RF radiation from lightning. *Journal of Geophysical Research: Oceans*, 85(C7), 4091-4095. doi: <https://doi.org/10.1029/JC085iC07p04091>
- Li, D., Azadifar, M., Rachidi, F., Rubinstein, M., Diendorfer, G., Sheshyekani, K., ... Wang, Z. (2016). Analysis of lightning electromagnetic field propagation in mountainous terrain and its effects on ToA-based lightning location systems. *Journal of Geophysical Research: Atmospheres*, 121(2), 895-911. doi: 10.1002/2015JD024234
- Li, D., Luque, A., Gordillo-Vazquez, F. J., Pérez-Invernón, F. J., Husbjerg, L. S., Neubert, T., ... Reglero, V. (2023). Different Types of Corona Discharges Associated With High-Altitude Positive Narrow Bipolar Events Nearby Cloud Top. *Journal of Geophysical Research: Atmospheres*, 128(4), e2022JD037883. doi: <https://doi.org/10.1029/2022JD037883>
- Li, D., Luque, A., Gordillo-Vázquez, F. J., Silva, C. d., Krehbiel, P. R., Rachidi, F., & Rubinstein, M. (2022). Secondary fast breakdown in narrow bipolar events. *Geophysical Research Letters*, 49(7), e2021GL097452. doi: <https://doi.org/10.1029/2021GL097452>
- Li, D., Luque, A., Lehtinen, N. G., Gordillo-Vázquez, F. J., Neubert, T., Lu, G., ... Reglero, V. (2022). Multi-Pulse Corona Discharges in Thunderclouds Observed in Optical and Radio Bands. *Geophysical Research Letters*, 49(13), e2022GL098938. doi: <https://doi.org/10.1029/2022GL098938>
- Li, D., Rubinstein, M., Rachidi, F., Diendorfer, G., Schulz, W., & Lu, G. (2017). Location Accuracy Evaluation of ToA-Based Lightning Location Systems Over Mountainous Terrain. *Journal of Geophysical Research: Atmospheres*, 122(21), 11,760-11,775. doi: 10.1002/2017JD027520
- Lyu, F., Cummer, S. A., Qin, Z., & Chen, M. (2019). Lightning Initiation Processes Imaged With Very High Frequency Broadband Interferometry. *Journal of Geophysical Research: Atmospheres*, 124(6), 2994-3004. doi: 10.1029/2018JD029817

- 361 Marshall, R. A., da Silva, C. L., & Pasko, V. P. (2015, July). Elve doublets and compact intracloud  
362 discharges. , *42*(14), 6112–6119. doi: 10.1002/2015GL064862
- 363 Marshall, T., Bandara, S., Karunarathne, N., Karunarathne, S., Kolmasova, I., Siedlecki, R., &  
364 Stolzenburg, M. (2019). A study of lightning flash initiation prior to the first initial breakdown  
365 pulse. *Atmospheric Research*, *217*, 10-23. doi: <https://doi.org/10.1016/j.atmosres.2018.10.013>
- 366 Marshall, T., Stolzenburg, M., Karunarathna, N., & Karunarathne, S. (2014). Electromagnetic activ-  
367 ity before initial breakdown pulses of lightning. *Journal of Geophysical Research: Atmospheres*,  
368 *119*(22), 12,558-12,574. doi: <https://doi.org/10.1002/2014JD022155>
- 369 Nag, A., & Rakov, V. A. (2010). Compact intracloud lightning discharges: 1. Mechanism of elec-  
370 tromagnetic radiation and modeling. *Journal of Geophysical Research: Atmospheres*, *115*(D20).  
371 doi: 10.1029/2010JD014235
- 372 Nucci, C. A., & Rachidi, F. (1989). Experimental validation of a modification to the Transmission  
373 Line model for LEMP calculation. In *8th symposium and technical exhibition on electromagnetic*  
374 *compatibility, zurich, switzerland*.
- 375 Phelps, C. (1974). Positive streamer system intensification and its possible role in lightning ini-  
376 tiation. *Journal of Atmospheric and Terrestrial Physics*, *36*(1), 103 - 111. doi: [https://doi.org/](https://doi.org/10.1016/0021-9169(74)90070-1)  
377 [10.1016/0021-9169\(74\)90070-1](https://doi.org/10.1016/0021-9169(74)90070-1)
- 378 Phelps, C., & Griffiths, R. F. (1976). Dependence of positive corona streamer propagation on air  
379 pressure and water vapor content. *Journal of Applied Physics*, *47*(7), 2929-2934. doi: 10.1063/  
380 1.323084
- 381 Rachidi, F., & Nucci, C. (1990). On the Master, Uman, Lin, Standler and the modified transmission  
382 line lightning return stroke current models. *Journal of Geophysical Research: Atmospheres*,  
383 *95*(D12), 20389-20393. doi: 10.1029/JD095iD12p20389
- 384 Rison, W., Krehbiel, P. R., Stock, M. G., Edens, H. E., Shao, X.-M., Thomas, R. J., ... Zhang, Y.  
385 (2016). Observations of narrow bipolar events reveal how lightning is initiated in thunderstorms.  
386 *Nature communications*, *7*, 10721. doi: 10.1038/ncomms10721(2016)
- 387 Rubinstein, M., & Uman, M. A. (1990). On the radiation field turn-on term associated with traveling  
388 current discontinuities in lightning. *Journal of Geophysical Research: Atmospheres*, *95*(D4),  
389 3711-3713. doi: 10.1029/JD095iD04p03711
- 390 Shao, X.-M., Fitzgerald, T. J., & Jacobson, A. R. (2005). Reply to comment by Rajeev Thottappillil  
391 and Vladimir A. Rakov on “Radio frequency radiation beam pattern of return strokes: A revisit to  
392 theoretical analysis”. *Journal of Geophysical Research: Atmospheres*, *110*(D24). doi: 10.1029/  
393 2005JD005889
- 394 Shao, X.-M., Jacobson, A. R., & Fitzgerald, T. J. (2004). Radio frequency radiation beam pattern  
395 of lightning return strokes: A revisit to theoretical analysis. *Journal of Geophysical Research:*  
396 *Atmospheres*, *109*(D19). doi: 10.1029/2004JD004612
- 397 Smith, D. A., Heavner, M. J., Jacobson, A. R., Shao, X. M., Massey, R. S., Sheldon, R. J., & Wiens,  
398 K. C. (2004). A method for determining intracloud lightning and ionospheric heights from  
399 VLF/LF electric field records. *Radio Science*, *39*(1), RS1010. doi: 10.1029/2002RS002790
- 400 Smith, D. A., Shao, X. M., Holden, D. N., Rhodes, C. T., Brook, M., Krehbiel, P. R., ... Thomas,  
401 R. J. (1999). A distinct class of isolated intracloud lightning discharges and their associated  
402 radio emissions. *Journal of Geophysical Research: Atmospheres*, *104*(D4), 4189-4212. doi:  
403 10.1029/1998JD200045
- 404 Thottappillil, R., & Rakov, V. (2001). On the computation of electric fields from a lightning dis-  
405 charge in time domain. In *2001 IEEE EMC international symposium on electromagnetic compat-*  
406 *ibility* (Vol. 2, pp. 1030–1035).
- 407 Thottappillil, R., & Rakov, V. A. (2005). Comment on “Radio frequency radiation beam pattern of  
408 lightning return strokes: A revisit to theoretical analysis” by Xuan-Min Shao, Abram R. Jacobson,  
409 and T. Joseph Fitzgerald, journal = *Journal of Geophysical Research: Atmospheres*. , *110*(D24).  
410 doi: 10.1029/2004JD005729
- 411 Thottappillil, R., Uman, M. A., & Rakov, V. A. (1998). Treatment of retardation effects in calcu-  
412 lating the radiated electromagnetic fields from the lightning discharge. *Journal of Geophysical*  
413 *Research: Atmospheres*, *103*(D8), 9003-9013. doi: 10.1029/97JD02941
- 414 Tilles, J. N., Liu, N., Stanley, M. A., Krehbiel, P. R., Rison, W., Stock, M. G., ... Wilson, J.

- 415 (2019). Fast negative breakdown in thunderstorms. *Nature communications*, 10(1), 1648. doi:  
416 10.1038/s41467-019-09621-z
- 417 Uman, M. A., & McLain, D. K. (1970). Radiation field and current of the lightning stepped  
418 leader. *Journal of Geophysical Research (1896-1977)*, 75(6), 1058-1066. doi: 10.1029/  
419 JC075i006p01058
- 420 Uman, M. A., McLain, D. K., & Krider, E. P. (1975). The electromagnetic radiation from a finite  
421 antenna. *American Journal of Physics*, 43(1), 33-38. doi: 10.1119/1.10027
- 422 Uman, M. A., Martin A., & McLain, D. K. (1970). Lightning return stroke current from magnetic  
423 and radiation field measurements. *Journal of Geophysical Research (1896-1977)*, 75(27), 5143-  
424 5147. doi: 10.1029/JC075i027p05143
- 425 Watson, S. S., & Marshall, T. C. (2007). Current propagation model for a narrow bipolar pulse.  
426 *Geophysical Research Letters*, 34(4). doi: 10.1029/2006GL027426

**Figure list**

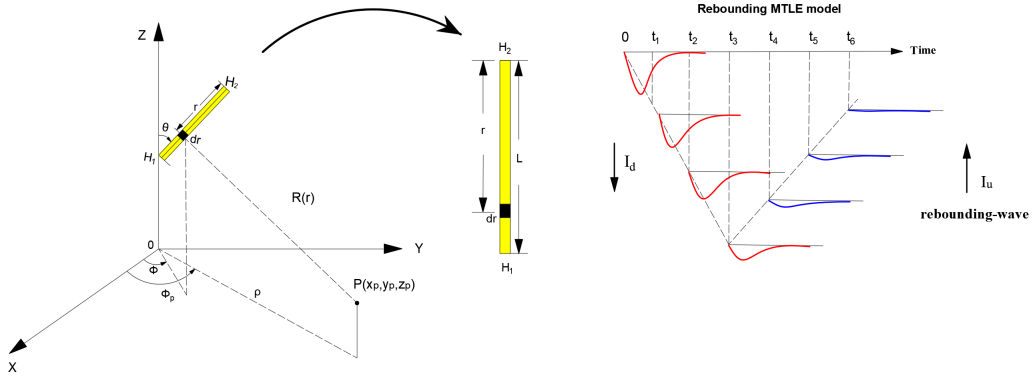


**Figure 1.** Geometry of the inclined NBE channel with a current that propagates following the rebounding MTLE model. (a) We model the NBE channel as a series of small straight segments at a radial distance of  $r$  and a polar angle  $\theta$  with respect to the Z axis. The azimuth angle  $\phi$  is defined by the angle between the X axis and the projection of the segment in the XY plane. The observation point  $P(x_p, y_p, z_p)$  is at an altitude  $z_p$  above the ground surface and at a plane distance  $\rho$  from the source, thus  $x_p = \rho \cos(\phi_p)$ ,  $y_p = \rho \sin(\phi_p)$ , where  $\phi_p$  is the azimuth angle of the observation point  $P$ . (b) In the rebounding MTLE model, the NBE channel is considered as a system of positive streamer coronas that propagate downward from an altitude  $H_2$  to  $H_1$  with a channel length  $L$ , followed by upward negative streamer corona discharges that propagate back along the same path. Here,  $I_d$  is the downward current and  $I_u$  is the rebounding-wave current.

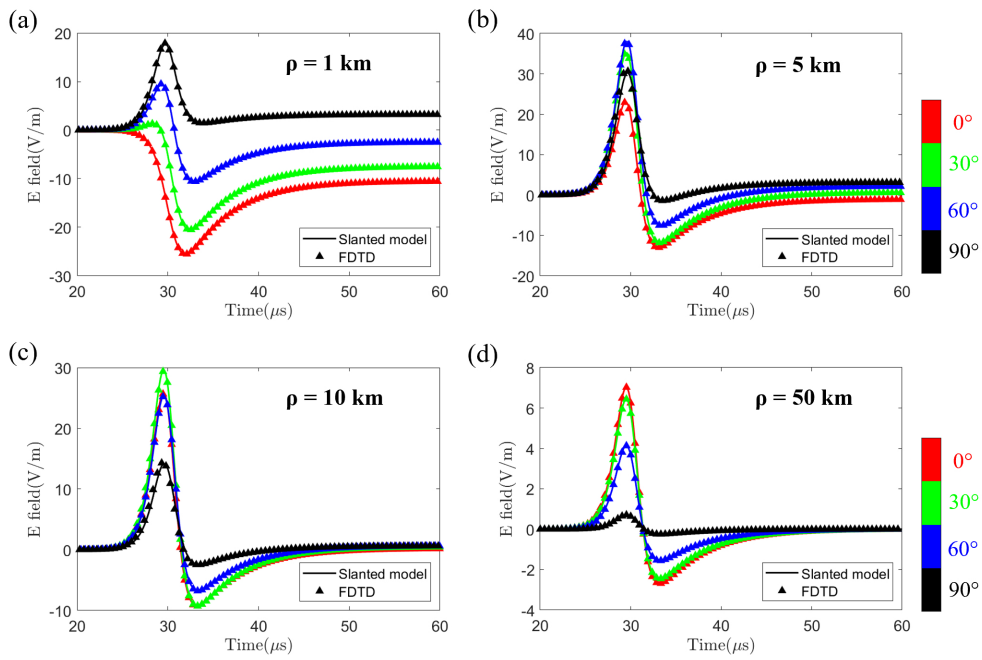


**Figure 2.** Comparison between the slanted rebounding wave model and FDTD method by considering the slanted dipole with different  $\theta$  angles with respect to the z-axis and the azimuthal angle  $\phi = 0^\circ$  at a distance of 1 km, 5 km, 10 km and 50 km.

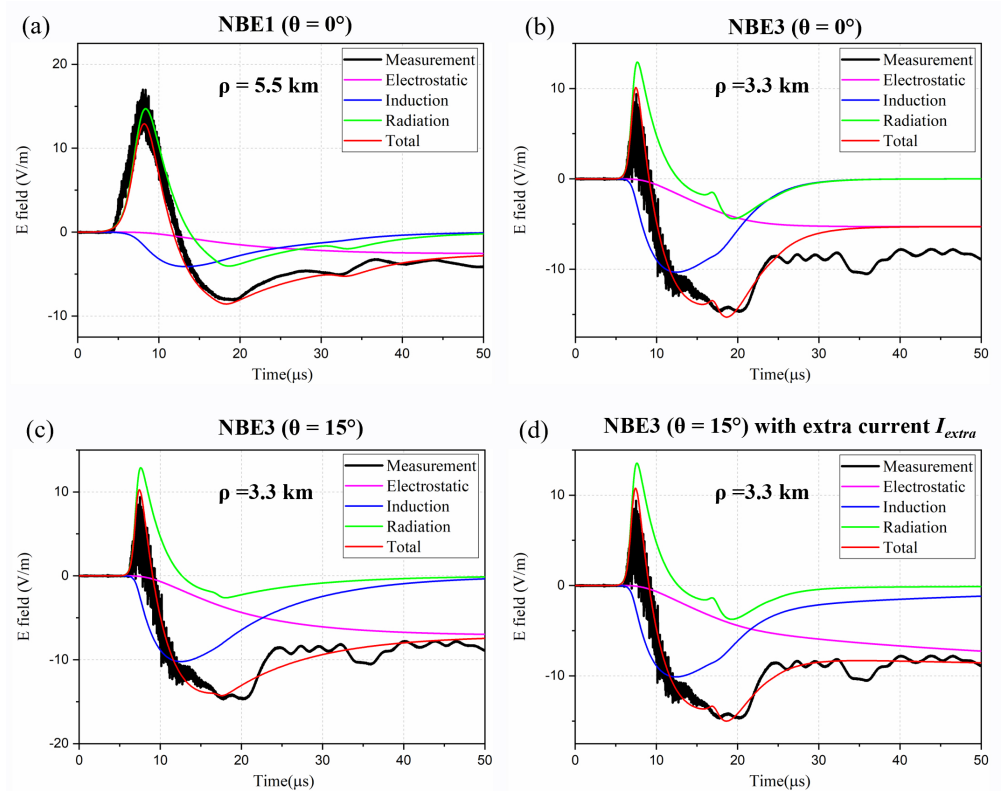


**Figure 3.** Comparison between the observations from Rison et al. (2016) and simulation results by assuming the vertical channel for NBE1(a) and NBE3(b) and the slanted channel for NBE3 without (c) and with (d) the extra current  $I_{extra}$ . The electrostatic, induction and radiation components of the total electric fields are also given in the figure.

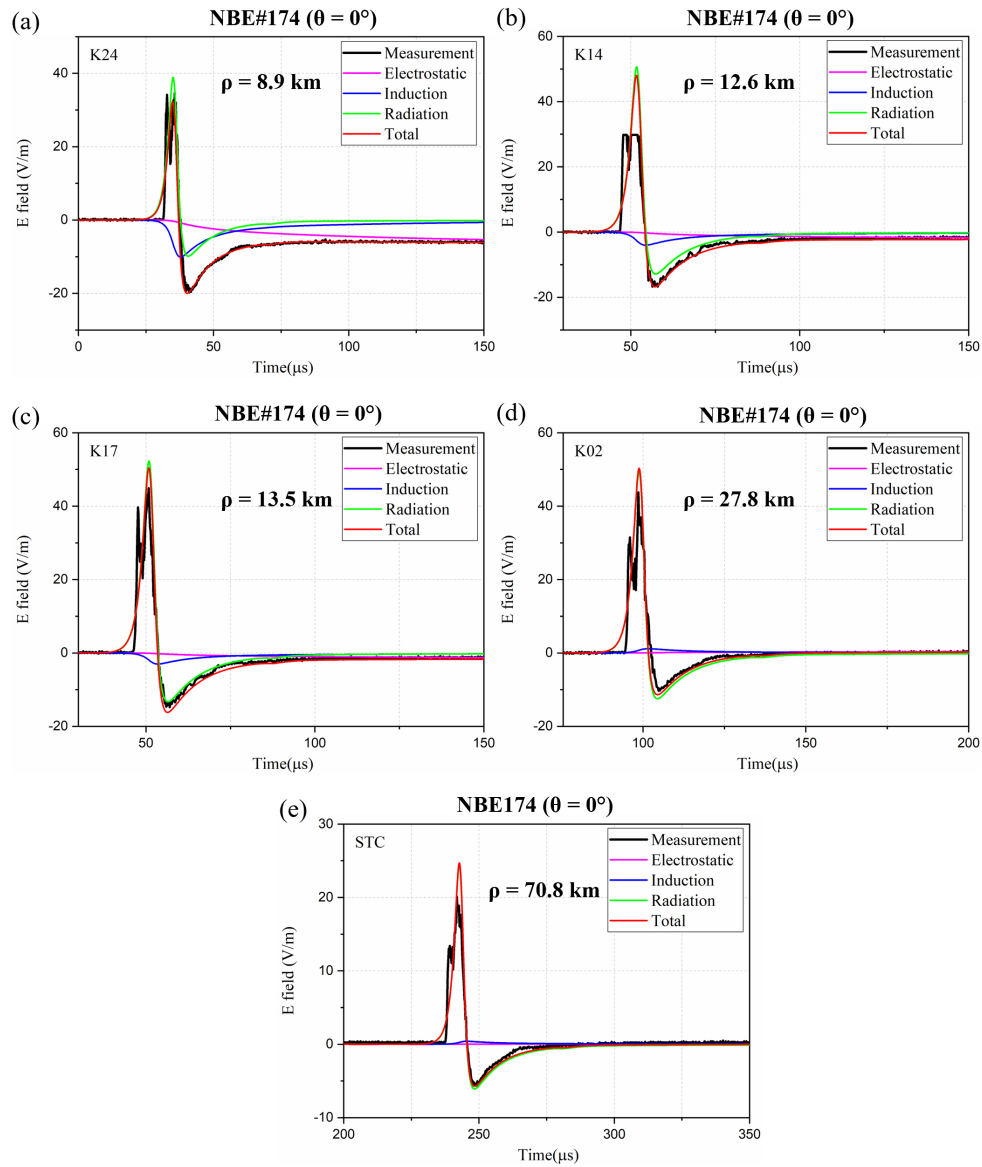


**Figure 4.** Comparison between the observations from Karunaratne et al. (2016) and simulation results by assuming a vertical channel for NBE#174 at different distances. The electrostatic, induction and radiation components of the total electric fields are also given in the figure.

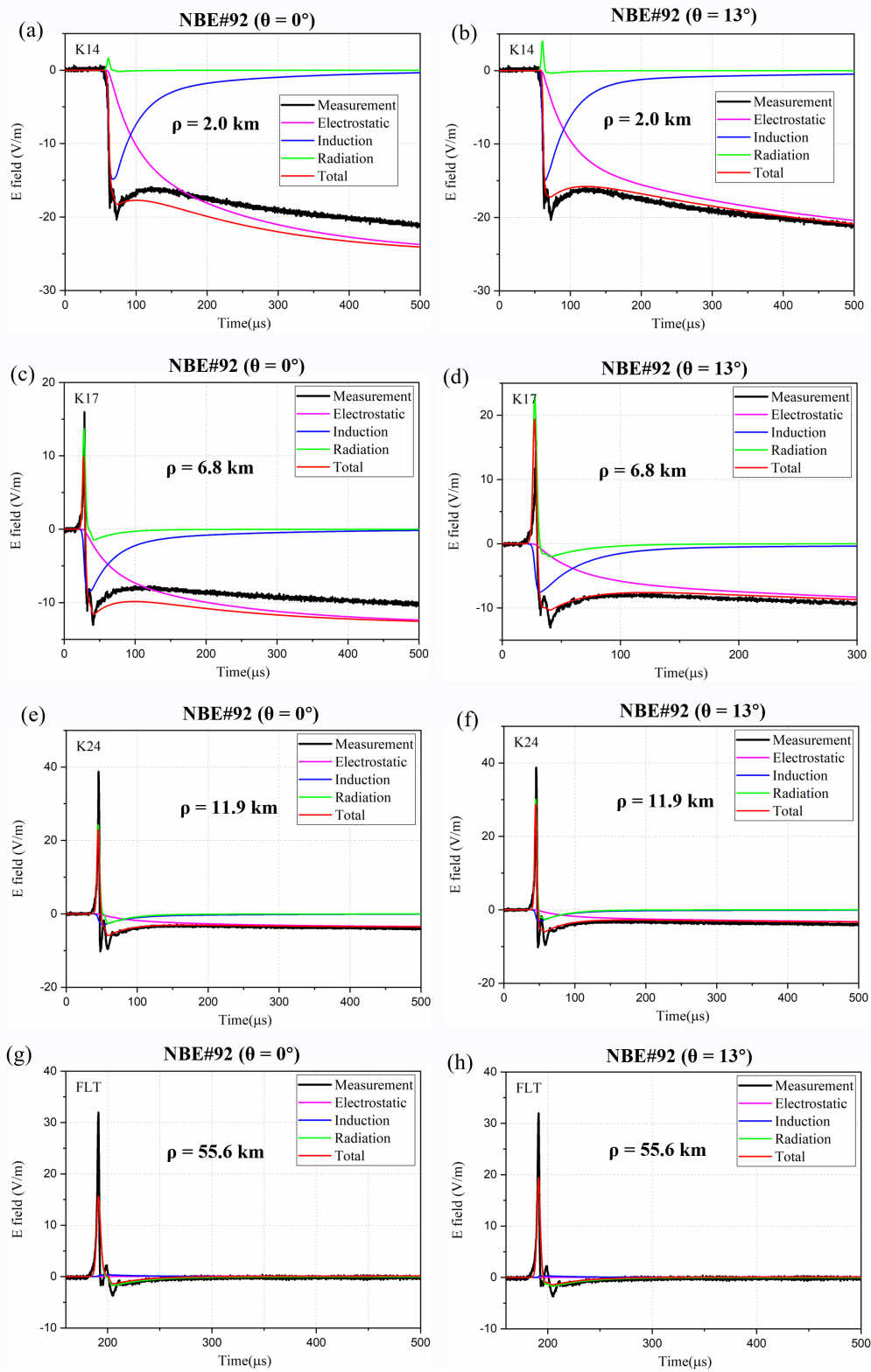


**Figure 5.** Comparison between the observations from Karunarathne et al. (2016) and simulation results by assuming a vertical channel (a,c,e,g) and a slanted channel (b,d,f,h) for NBE#92 at different distances. The electrostatic, induction and radiation components of the total electric fields are also given in the figure.